Supporting Information for

Anisotropic Silicon-Modified Loofah Carbon Aerogels for Synergistic Solar-Environmental Energy Harvesting in Interfacial Evaporation

Wentao Zhu,[a,b] *Yi Jin,*[b] *and Jiangang Yu**[b]

[a]College of Chemical Engineering, Zhejiang University of Technology, Hangzhou 310014, PR China

[b]College of Chemical and Material Engineering, Quzhou University, Quzhou 324000, PR China

E-mail: jgyu@qzc.edu.cn

Contents

Calculation of Evaporation Rate [1-3]

The evaporation rate (v) is estimated by (1), which unit is kg $m^{-2}\cdot h^{-1}$.

$$v = \Delta m/A \tag{1}$$

where Δm ($kg\cdot h^{-1}$) is the mass change per hour of the evaporation system, A (m^2) is the projection area of sample.

Theoretical Foundation of the Energy Balance Model[4,5]

The model adheres to the principle of energy conservation. Under conditions of steady-state evaporation, the total energy absorbed by the solar evaporator system is equivalent to the aggregate of energy losses and the energy expended for the purpose of water evaporation.

The energy balance equation can be expressed as:

$$Q_{in} = Q_{out} + Q_{evaporation} \tag{2}$$

where Q_{in} is the total energy input to the system. Q_{out} is the total heat loss from the system. $Q_{evaporation}$ is the useful energy used for water evaporation.

To ensure the comprehensiveness of the model, it is imperative to conduct a detailed mathematical analysis of each energy component.

The total energy input to the system consists of two main parts: solar energy absorption and environmental energy harvesting.

$$Q_{in} = Q_{solar} + Q_{ambient} \tag{3}$$

where Q_{solar} is the energy provided by solar irradiance absorbed by the top surface of the evaporator.

$$Q_{solar} = \alpha\cdot P_{solar}\cdot A_{top} \tag{4}$$

where α is the average solar absorptivity of the evaporator's top surface, which is 96.4% for C-P_3T. P_{solar} is the solar irradiance (e.g., 1 sun = 1000 W/m²). A_{top} is the surface area of the evaporator's top.

Ambient energy farvesting ($Q_{ambient}$) comes from convective heat transfer at the side surfaces of the evaporator. The evaporator's side surfaces are cooled to below ambient temperature via radiative cooling, which drives a net heat influx from the surroundings.

$$Q_{ambient} = Q_{convection,side} = h_{conv}\cdot A_{side}\cdot(T_{amb} - T_{side}) \tag{5}$$

where h_{conv} is the convective heat transfer coefficient (assumed to be 10 $W\cdot m^{-2}\cdot K^{-1}$) [4]. A_{side} is the surface area of the evaporator's side. T_{amb} is the ambient temperature, measured in real-time by infrared thermography. T_{side} is the temperature of the evaporator's side surface.

The efficiency of solar-steam conversion ($\eta_{apparent}$) is estimated by (6).

(6)

where $\dot{m}$ ($kg\cdot m^{-2}\cdot h^{-1}$) denotes the net evaporation rate of the sample under illumination ($\dot{m} = v_{light} - v_{dark}$), H_{LV} is the latent heat of the water (~ 2256 $kJ\cdot kg^{-1}$), C_{opt} is the optical concentration, q_0 is the light intensity of one sun (1 $kw\cdot m^{-2}$). Q refers to the sensible heat of water, which can be calculated by (7).

$$Q = c \times (T_1 - T_0) \quad (7)$$

where T_1 represented the temperature of evaporation (K). T_0 represented the initial temperature of the water (K). where c (4.2 kJ·kg^{-1}·K^{-1}) is the specific heat of water and ΔT (K) is the temperature difference before and after evaporation.

The contribution of environmental energy to the total input energy was calculated during the harvesting process.

$$\eta_{enc} = \frac{Q_{ambient}}{Q_{In}} \times 100\% \quad (8)$$

Calculation of the crystallite size (D) the microstrain (ε) [6]

$$D = \frac{k\lambda}{\beta \cos\theta} \quad (9)$$

$$\varepsilon = \frac{\beta}{(4\tan\theta)} \quad (10)$$

where k is the constant (k = 0.89), θ is the Bragg diffraction angle, λ is the X-ray source wavelength (λ = 1.54056 Å), and β is the full width at half maximum (FWHM).

Calculation of the porosity of evaporators

$$\varphi = \frac{m_1 - m_2}{V\rho} \quad (11)$$

where m_1 and m_2 are the mass of the evaporators before and after full absorption of water (kg), respectively, V is the volume of the evaporator (m^3), ρ is the density of the water (kg·m^{-3}).

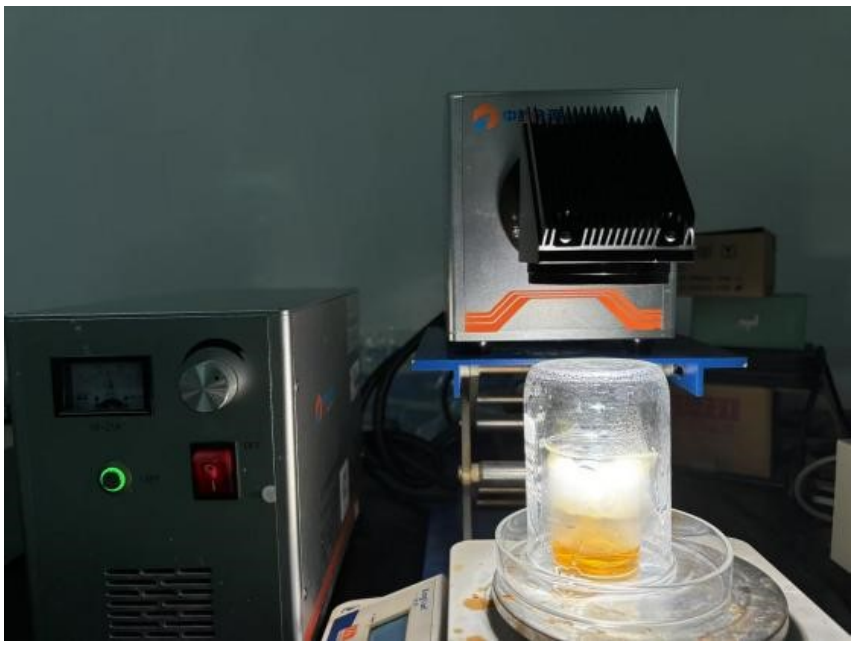

Fig. S1 The schematic diagram of solar driven evaporation device.

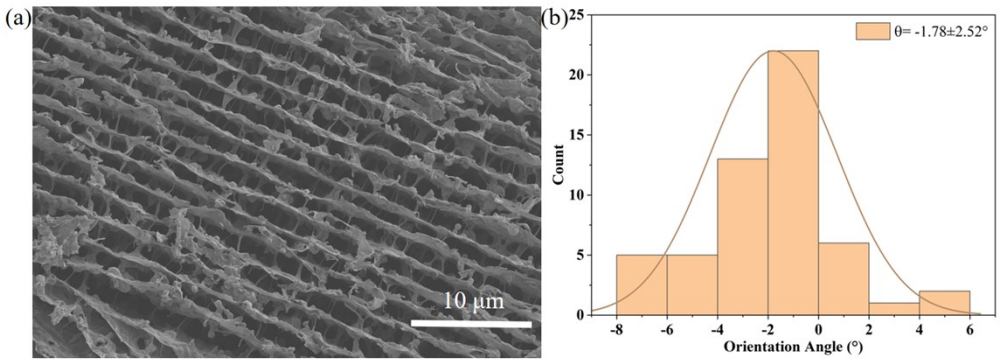

Fig. S2 (a) Cross-sectional SEM image of C-P_2T, (b) quantitative statistical distribution of the channel orientation angles calculated from SEM analysis.

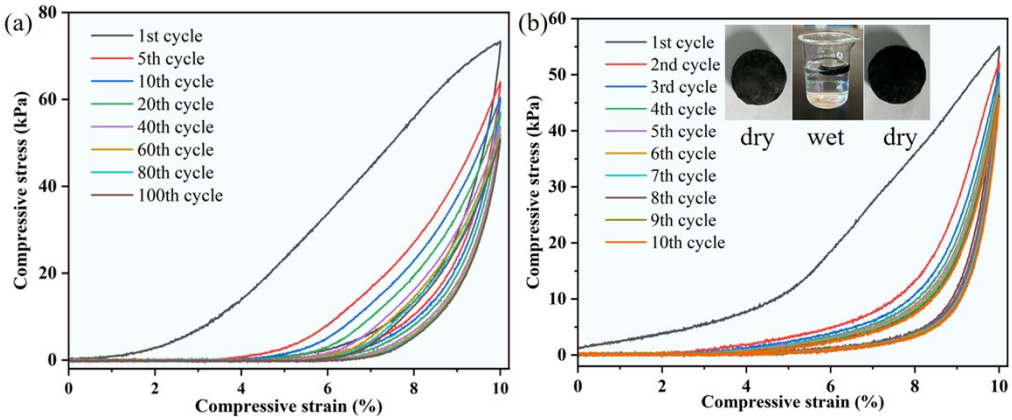

Fig. S3 Stability evaluation of the C-P_3T aerogel. (a) Cyclic compressive stress-strain curves for 100 cycles at a fixed 10% strain (rate: 1 mm·min^{-1}), (b) compressive cycling tests (10 cycles) performed on the aerogel after being subjected to water immersion and drying (wet-dry cycles).

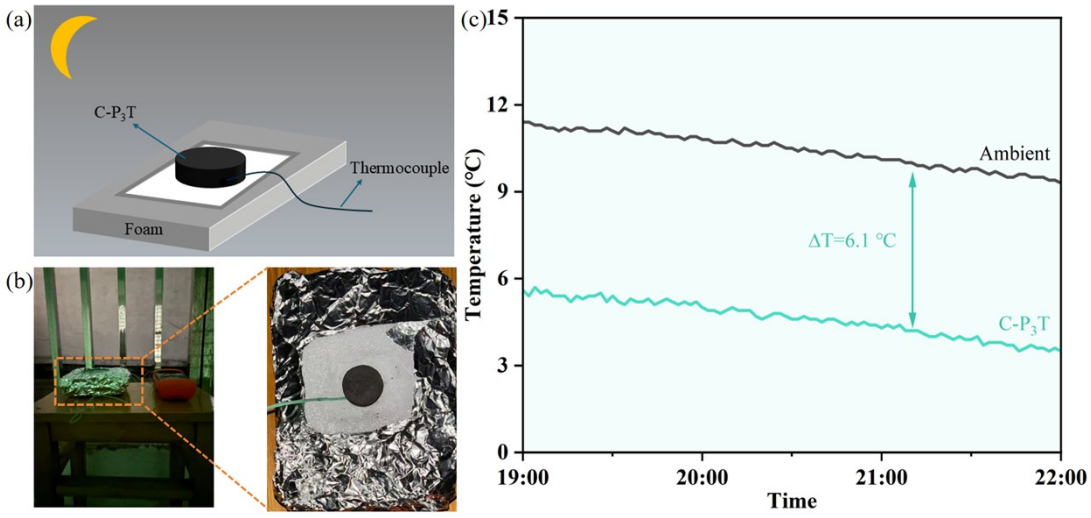

Fig. S4 (a) Schematic illustration of the setup used to evaluate the night-time passive radiative cooling performance, (b) photograph of the outdoor experimental setup with the aerogel mounted on insulation foam, (c) real-time temperature measurement of the C-P_3T aerogel and ambient air from 19:00 to 22:00, showing a sub-ambient cooling ΔT of ≈ 6.1 °C.

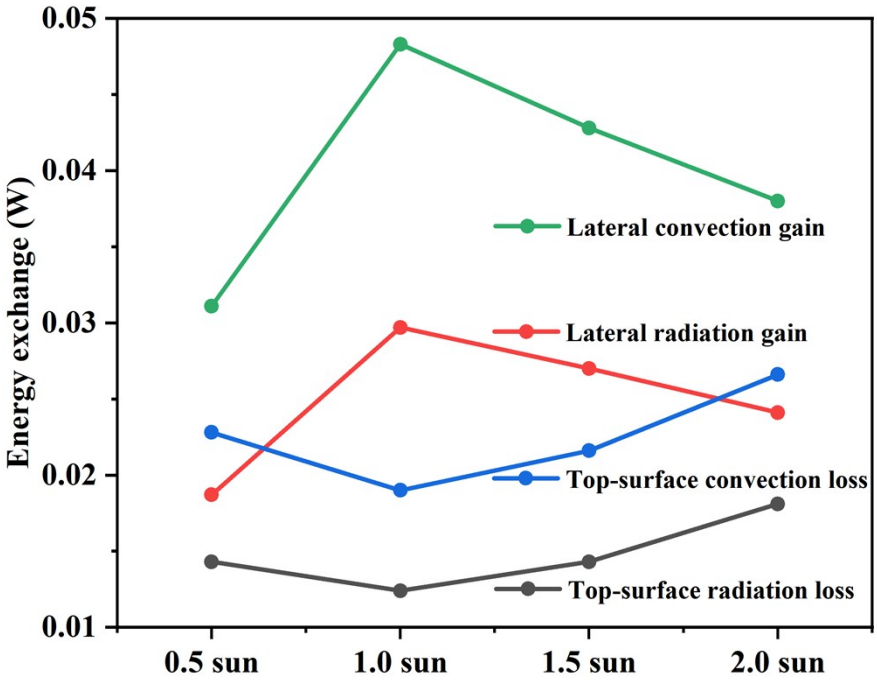

Fig. S5 Energy exchange between the carbon aerogel and environment under different sunlight intensities.

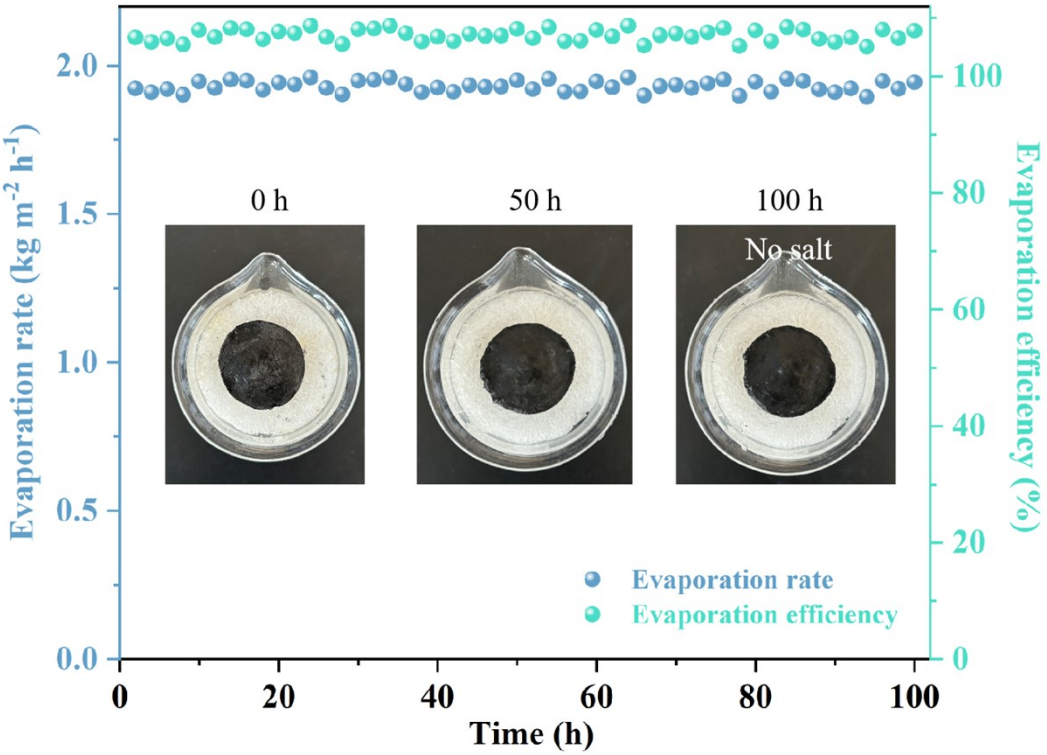

Fig. S6 The solar evaporation experiment of the C-P_3T aerogel to continuous 100 h in 3.5 wt% NaCl solution under 1 sun illumination.

References

[1] Noureen, L., Wang, Q., Ismail, P.M., Alomar, M., Arshad, N., Irshad, M.S., Xu, Q.Y. and Wang, X.W. (2024) Multifunctional aerogel with antibiofouling properties for efficient solar

steam generation and seawater desalination. Nano Today 54, 102130.

[2] Li, W., Tian, X.H., Li, X.F., Liu, J., Li, C.J., Feng, X.Y., Shu, C. and Yu, Z.Z. (2022) An environmental energy-enhanced solar steam evaporator derived from MXene-decorated cellulose acetate cigarette filter with ultrahigh solar steam generation efficiency. Journal of Colloid and Interface Science 606, 748-757.

[3] Zhou, H., Xue, J., Che, Q.L., Kong, L.F., Zhang, N.N., Tao, C.Y. and Fan, X. (2023) Rollable and Ventilated Net-Based Solar Thermal Water Evaporator for Casting on Water Surface. Small Structures 4(7), 2300008.

[4] Duan, H.Y., Wang, M.X., Zhang, Z.W., Zhen, J.Z. and Lv, W.Y. (2023) Biomass-derived photothermal carbon aerogel for efficient solar-driven seawater desalination. Journal of Environmental Chemical Engineering 11(2), 109295.

[5] Ming, Y., Shi, S., Cai, W., Liu, J., Chen, D.M., Hu, X., Yu, R.J., Zhou, X., Tawiah, B. and Fei, B. (2025) A scalable wood-based interfacial evaporator assisted with localized joule heating for round-the-clock operations. Chemical Engineering Journal 504, 158690.

[6] Yu, J., Bao, P., Liu, J., Jin, Y., Li, J. and Lv, Y. (2023) Cu and Ni dual-doped ZnO nanostructures templated by cellulose nanofibrils for the boosted visible-light photocatalytic degradation of wastewater pollutants. Green Chemistry 25(24), 10530-10537.